

# Mechanism of growth reduction of the deceleration-phase ablative Rayleigh-Taylor instability

Stefano Atzeni<sup>1</sup> and Mauro Temporal<sup>2</sup><sup>1</sup>*Dipartimento di Energetica, Università di Roma "La Sapienza" and INFN, Via Antonio Scarpa 14, I-00161 Roma, Italy*<sup>2</sup>*ETSII, Universidad de Castilla-La Mancha, Ciudad Real, Spain*

(Received 13 November 2002; published 9 May 2003)

The deceleration-phase (dp) ablative Rayleigh-Taylor instability (RTI) of igniting and nonigniting inertial fusion capsules is studied by high-resolution two-dimensional Lagrangian fluid simulations. It is found that growth reduction of the dp-RTI with respect to classical RTI results from the advection of perturbed fluid elements outside a thin unstable fluid layer. Within this layer, at fixed Lagrangian position, perturbations grow approximately classically.

DOI: 10.1103/PhysRevE.67.057401

PACS number(s): 52.35.Py, 47.20.-k, 52.57.Fg

The Rayleigh-Taylor instability [1,2] occurs when a denser fluid layer is accelerated by a lighter fluid. RTIs occur in astrophysics [3], geophysics [4], and inertial confinement fusion (ICF) [5]. In these cases, however, several processes, and in particular, intense energy flow, modify the classical RTI described in Refs. [1,2] (see Ref. [6] for an extensive review).

In ICF, a spherical shell containing cryogenic deuterium-tritium (DT) fuel and filled with DT vapor is imploded and compressed to very high density by laser or x-ray irradiation. A first RTI then develops at the outer shell surface, during the stage of ablation driven implosion. Theoretical [6–9], numerical [10–12], and experimental [13,14] studies show that the growth of the relevant *ablative* RTI is reduced with respect to the classical rate. The linear growth rates from two-dimensional (2D) numerical simulations [11,12] and experiments [13] approximately agree with the relation [5,15]

$$\gamma = \alpha \sqrt{\frac{gk}{1 + kL_m}} - \beta k u_a, \quad (1)$$

which generalizes earlier expressions by Bodner [7] and Takabe [8]. In Eq. (1),  $k$  is the wave number,  $g$  is the acceleration,  $L_m$  is the minimum value of the density scale length  $L = \rho/\nabla\rho$  at the ablation front,  $u_a$  is the ablation velocity, and  $\alpha$  and  $\beta$  are numerical coefficients depending on the flow parameters [15], and typically varying in the ranges  $\alpha = 0.9\text{--}0.95$  and  $\beta = 1\text{--}3$ . When the imploding shell is slowed down by the high pressure exerted by the inner DT gas *hot spot*, the so-called deceleration phase RTI (dp-RTI) develops at the inner shell surface [16]. At this time, dense shell material is ablated by the energy flux carried by electrons and 3.5-MeV fusion  $\alpha$  particles leaving the hot spot [17]. Recently, Lobatchev and Betti [18] pointed out the beneficial effect of ablation on the dp-RTI, the linear growth rate of which can still be approximated by Eq. (1). Measurements of dp-RTI growth have been reported in Ref. [19].

Despite the above mentioned research, as well as major progress in nonlinear theories [20], understanding of the linear stage of the ablative RTI is still incomplete, e.g., mode structure and evolution of the perturbed flow have not been analyzed in detail.

In this paper, we present results of high-resolution 2D Lagrangian simulations which provide insight into the stabilization mechanism of the dp-RTI, and more generally, of the

ablative RTI. In particular, we analyze the structure and location of the perturbation modes, and study the development of the perturbation at fixed Lagrangian positions. We conclude that perturbations grow approximately classically in the dense fluid layer close to the unstable surface, and growth is limited by advection of the perturbed fluid outside such a layer.

Our study refers to an ICF shell capsule with parameters similar to those of the indirect-drive point design for the National Ignition Facility (Ref. [5], p. 4009). The shell has outer radius of 1.1 mm and inner radius of 0.87 mm; it consists of a layer of Br-doped plastics and an inner 0.2-mg DT layer, and contains DT vapor with a density of  $4 \times 10^{-4}$  g/cm<sup>3</sup>. According to one-dimensional (1D) simulations, the fuel ignites and releases 14 MJ of fusion energy when the shell is driven by a time-shaped pulse of thermal x rays with total energy of 150 kJ and about 300-eV peak temperature. We have simulated the dp-RTI of this capsule by the 2D Lagrangian fluid code DUED [21]. This code includes a two-temperature model with classical flux-limited conductivities, a real-matter equation of state, DT fusion reactions, single-group time-dependent diffusion of  $\alpha$ -particle energy, and  $\alpha$ -particle contribution to fluid pressure. As in Ref. [18] (see also the discussion in Ref. [22]) we assume bremsstrahlung loss from the hot spot and neglect radiative transfer. The 2D simulations start (time  $t=0$ ) about 100 ps before beginning of shell deceleration, and take as initial conditions the output of a run by the 1D code SARA [23]. A small 2D perturbation is introduced as a single-mode radial displacement centered around the hot spot surface:  $\delta R(r, \theta, t=0) = A(r, t=0) P_l(\cos \theta)$ , with  $A(r, t=0) = A_0 \exp[-l|r - R_{h0}|/R_{h0}]$ , where  $l$  is the mode number,  $P_l$  is the Legendre polynomial of order  $l$ ,  $\theta$  is the angle between the cylindrical symmetry axis and the radial direction,  $R_{h0} = R_h(t=0)$  is the radius of hot spot (taken as the location of the minimum density scale length). Code mesh is uniform in  $\theta$  (with  $3l\text{--}6l$  points in a 90° sector) and non-uniform in  $r$  (with typically 170 points for the DT region, with very fine spacing in the region close to the hot spot boundary). According to previous experience with DUED [12], at least for  $l \leq 80$ , growth rates computed with the adopted mesh should be (90–95)% of the theoretical values. Figure 1(a) shows the 1D flow chart for this problem, computed by DUED assuming perfect spherical symmetry. The dashed curves indicate the boundaries of the initially cryo-

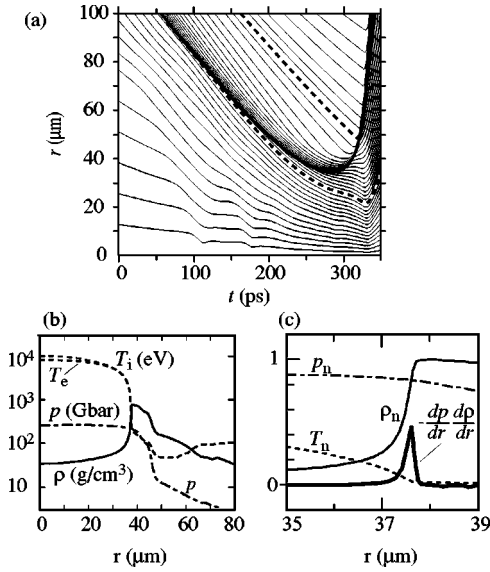


FIG. 1. (a) 1D flow chart of the final stage of implosion; the thin curves represent  $r-t$  trajectories of selected Lagrangian mesh points; (b) and (c) radial profiles at  $t=250$  ps. In (c) density, pressure, and temperature are normalized to peak values;  $-(dp/dr)(d\rho/dr)$  is in arbitrary units.

genic fuel; curves are denser at the hot spot front. The coasting shell starts decelerating about  $t=100$  ps. Ignition occurs about  $t=290$  ps, and is followed by the propagating burn. Figure 1(b) shows radial profiles of density  $\rho$ , ion temperature and pressure  $p$ , at time  $t=250$  ps, when the hot spot radius is  $R_h=37.5 \mu\text{m}$ . A zoom of the same profiles around  $R_h$  is shown in Fig. 1(c). The most unstable region is the thin layer where the product  $-(dp/dr)(d\rho/dr)$  peaks [2].

Due to ablation (see the hot spot front moving into the shell), the acceleration of the hot spot surface  $d^2R_h/dt^2$  differs from the acceleration  $g$  of the fluid element at  $r=R_h$ . In the interval  $200 \leq t \leq 290$  ps the latter increases from 1.5 to  $5.2 \times 10^{17} \text{ cm/s}^2$ . In the same time interval, the ablation velocity (ratio of the areal mass ablation rate to the peak density) increases from 0.7 to  $1.6 \times 10^6 \text{ cm/s}$ , while the density scale length is roughly constant,  $L_m \approx 0.4 \mu\text{m}$ .

We now discuss 2D results. In the linear stage, perturbations (i.e., deformations of the Lagrangian mesh) have the form  $\delta R(r, \theta, t) = A(r, t)P_l(\cos \theta)$ . Figures 2(a) and 2(b) show perturbation amplitude  $A$  vs radius, at selected times, for cases with  $l=8$  and  $l=56$ , respectively; Fig. 2(c) presents the radial density profiles at the same times. Unlike the classical nonablative case, in which the mode peaks at the unstable interface [1], here  $A(r)$  peaks in the ablated fluid, at  $r=R_{\text{peak}}=R_h-\Delta R$ . For a given  $l$ ,  $\Delta R$  grows in time with  $u_a$ . At times close to stagnation,  $\Delta R$  approximately scale as  $\Delta R \propto 1/l^{1/2}$ , for  $l \leq 96$  (a detailed analysis will be presented elsewhere).

Since fluid is ablated, the perturbation peaks, at any time, at a different fluid element. This is clear from Fig. 3(a), showing the evolution of the perturbation  $A_i(t) = A[r_i(t), t]$  at selected Lagrangian locations (labeled by the index  $i$ ), for a run with  $l=48$ . Solid curves correspond to fluid elements

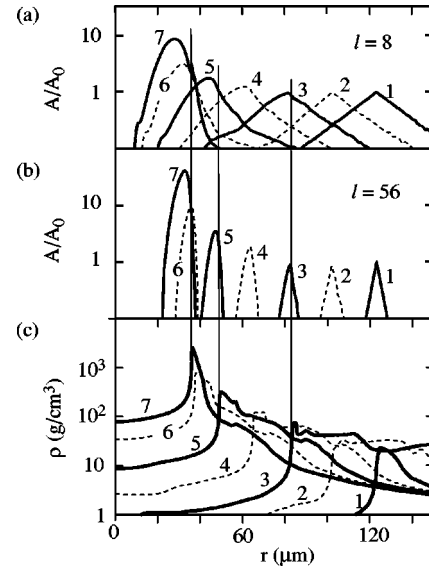


FIG. 2. (a) and (b) Perturbation amplitude vs radius at selected times, for mode numbers  $l=8$  and  $l=56$ ; (c) density profiles at the same times. The thin vertical lines indicate the location  $r=R_h$  of the hot spot front at time levels (3), (5), and (7). (1)  $t=0$ , (2)  $t=50$  ps, (3)  $t=100$  ps, (4)  $t=150$  ps, (5)  $t=200$  ps, (6)  $t=250$  ps, (7)  $t=300$  ps.

initially laying in the dense shell, while dashed curves refer to elements already in the gas at  $t=0$ . The thick dashed curve shows  $A[r=R_h(t)]$  at the hot spot front. Perturbations start growing at  $t \approx 100$  ps, when deceleration begins. The following evolution is rather complex. However [see the thick solid curves in Fig. 3(b)], growth is nearly exponential when the fluid element is still in the shell; it continues at

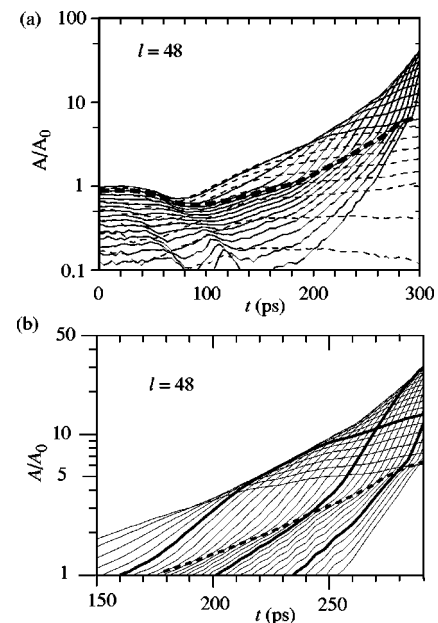


FIG. 3. Perturbation amplitude vs time at selected Lagrangian locations, for a case with  $l=48$ . In (a) we plot the perturbation amplitude at each second Lagrangian point; in (b) at each point initially laying in the shell.

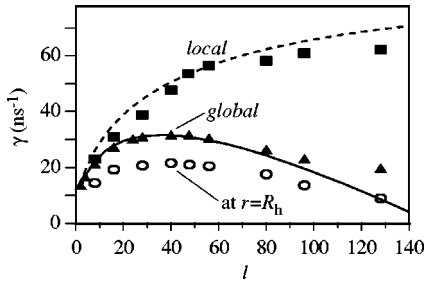


FIG. 4. Linear growth rate vs mode number. Squares, *local* growth rate at  $t=270$  ps; triangles, *global* mode growth rate; circles, growth rate of the perturbation at  $r=R_h$ . Curves: Eq. (1), with flow parameters as in the main text.

larger rate as the element is ablated and expands, and then decreases sharply as the advected element exits the most unstable region. The above observations suggest us to define a *local* growth rate  $\gamma_{loc} = d \ln A_{i^*} / dt$ , referring to Lagrangian elements  $i^*$  in a region of the dense shell close to the unstable surface, i.e., just below the thick dashed curve of Fig. 3(b). In addition, we consider the *global* growth rate  $\gamma = d \ln(\max_i[A_i(t)]) / dt$  of the peak of the perturbation, represented by the envelope of the curves of Fig. 3. (Alternative definitions of the growth rate can also be considered, referring, for instance, to the perturbation of the hot spot boundary, or to the areal mass perturbation  $\int \rho dr$  [14].) Local growth rates computed at time  $t=270$  ps are plotted in Fig. 4 vs mode number  $l$  (squares) [25]. These data compare well with the dispersion curve (dashed) obtained from Eq. (1), setting  $\alpha=0.95$ ,  $k=l/R_h$ , using the values  $g=3.6 \times 10^{17}$  cm/s<sup>2</sup>,  $L_m=0.4$   $\mu$ m, and  $R_h=34.7$   $\mu$ m, given by the simulations at the same time  $t=270$  ps, and neglecting ablation ( $u_a=0$ ). Global growth rates in the interval  $250 \leq t \leq 290$  ps are also shown (triangles) in the same figure. For  $l \leq 96$  they agree well with Eq. (1), with time averaged  $\beta u_a = 1.65 \times 10^6$  cm/s, and the same values of  $g$ ,  $L_m$ , and  $R_h$  as before. Significant deviations, instead, appear for  $l=128$ . Figure 4 also shows (circles) growth rates for the perturbation amplitude at the hot spot boundary. The above analysis shows that perturbations grow classically in the unstable layer; growth reduction of the global perturbation results from advection of the perturbed fluid layers. These results

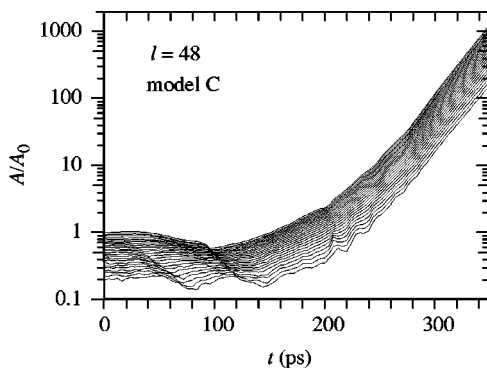


FIG. 5. Same as Fig. 3, but for a simulation with model C. Only amplitudes at Lagrangian points in the dense shell are plotted. Growth of the perturbation in the gas is analogous.

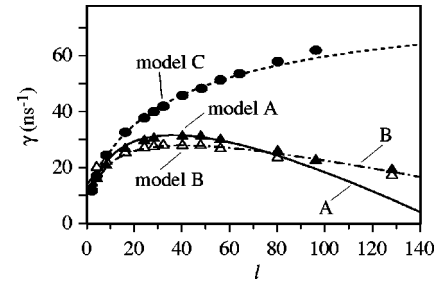


FIG. 6. *Global* growth rates from 2D simulations (symbols) and dispersion curves computed by Eq. (1) for the three different simulation models. Data refer in each case to time intervals just before stagnation:  $t=250$ – $290$  ps (model A),  $t=320$ – $360$  ps (model B), and  $t=230$ – $330$  ps (model C), respectively.

support quantitatively the explanation for ablative stabilization first proposed by Lindl (see Ref. [24], p. 1382, and Ref. [5], p. 3962).

In addition to the simulations with the above physical model (model A in the following), we have run DUED taking the same initial conditions, but neglecting fusion reactions (model B), and neglecting both fusion reactions and electron thermal conductivity (model C). In these cases  $g$ ,  $u_a$ , and  $L_m$  are nearly constant in the time interval  $200 \leq t \leq 400$  ps. In model B,  $g=2.1 \times 10^{17}$  cm/s<sup>2</sup>,  $u_a \approx 3 \times 10^5$  cm/s,  $L_h \approx 0.9$   $\mu$ m; in model C,  $g=2.5 \times 10^{17}$  cm/s<sup>2</sup>,  $u_a=0$ ,  $L_h \approx 0.4$   $\mu$ m. Shell stagnation occurs at  $t=360$  ps in model B and at  $t=320$  ps in model C.

Simulations with model C show that modes are *frozen* in the fluid and growth of perturbations is practically the same at all Lagrangian locations (see Fig. 5), and exponential in the interval  $250 \leq t \leq 350$  ps. Growth rates, shown in Fig. 6, agree with the scaling  $\gamma \approx \sqrt{gk/(1+kL_m)}$ . Comparison of these rates with model-A global rates show that dp-RTI ablative growth rates are much smaller than the nonablative ones, despite the much stronger acceleration.

Model-B simulations yield global growth rates (see Fig. 6) analogous to those computed from model A, and in agreement with Eq. (1), with values of the flow parameters taken from 1D simulations. Notice that the performance of a real ICF shell should be intermediate between model-A and model-B computations, because departures from ideal behavior are likely to result in delayed ignition. According to our results, dp-RTI growth is rather insensitive to hot spot evolution. However, in case of retarded ignition, RTI has longer time to grow.

In summary, 2D simulations confirm ablative stabilization of the dp-RTI, show approximately classical local growth in the unstable layer, and global growth reduction caused by advection. Future studies should also consider other measures of instability growth, and include radiative transfer and more accurate treatments of  $\alpha$ -particle transport.

We thank J. J. Honrubia for providing us output data from a SARA simulation. M.T. acknowledges useful discussions with R. Piriz. This work was supported by the Ministero per l'Istruzione, l'Università e la Ricerca (MIUR, Italy) and by the Ministerio de Ciencia y Tecnología of Spain (Grant No. FTN-2000-2048-C03-02).

- [1] Lord Rayleigh, *Scientific Papers, Vol. II* (Cambridge University Press, Cambridge, 1900), p. 200; G.I. Taylor, Proc. R. Soc. London, Ser. A **201**, 192 (1950).
- [2] S. Chandrasekhar, *Hydrodynamic and Hydromagnetic Stability* (Oxford University Press, Glasgow, 1961).
- [3] L. Smarr *et al.*, *Astrophys. J.* **246**, 515 (1981); W.D. Arnett *et al.*, *Annu. Rev. Astron. Astrophys.* **27**, 629 (1989); A. Burrows and B.A. Fryxell, *Science* (Washington, DC, U.S.) **258**, 430 (1992).
- [4] F. Selig and E.G. Wermund, *Geophysics* **32**, 726 (1966).
- [5] J.D. Lindl, *Phys. Plasmas* **2**, 3933 (1995).
- [6] H.J. Kull, *Phys. Rep.* **206**, 199 (1991).
- [7] S. Bodner, *Phys. Rev. Lett.* **33**, 761 (1974).
- [8] H. Takabe *et al.*, *Phys. Fluids* **25**, 1653 (1982).
- [9] J. Sanz, *Phys. Rev. Lett.* **73**, 2700 (1994); *Phys. Rev. E* **53**, 4026 (1996); R. Betti *et al.*, *Phys. Plasmas* **3**, 2122 (1996); V. Goncharov *et al.*, *ibid.* **3**, 4665 (1996); A.R. Piriz *et al.*, *ibid.* **1**, 1117 (1997).
- [10] J.D. Lindl and W.C. Mead, *Phys. Rev. Lett.* **34**, 1273 (1975); C.P. Verdon *et al.*, *Phys. Fluids* **25**, 1653 (1982); K.O. Mikaelian, *Phys. Rev. A* **42**, 4944 (1990); J.P. Dahlburg and J.H. Gardner, *ibid.* **41**, 5695 (1990).
- [11] M. Tabak *et al.*, *Phys. Fluids B* **2**, 1007 (1990); J.H. Gardner *et al.*, *ibid.* **3**, 1071 (1990).
- [12] S. Atzeni, *Nucl. Fusion* **36**, 69 (1996).
- [13] M. Desselberger *et al.*, *Phys. Rev. Lett.* **65**, 2997 (1990); B.A. Remington *et al.*, *ibid.* **67**, 3259 (1991); S.V. Weber *et al.*, *Phys. Plasmas* **1**, 3652 (1994); K.S. Budil *et al.*, *Phys. Rev. Lett.* **76**, 4536 (1996); S.G. Glendinning *et al.*, *ibid.* **78**, 3318 (1997); K.S. Budil *et al.*, *Phys. Plasmas* **8**, 2344 (2001); T. Sakaiya *et al.*, *Phys. Rev. Lett.* **88**, 145003 (2002).
- [14] J.P. Knauer *et al.*, *Phys. Plasmas* **7**, 338 (2000).
- [15] R. Betti *et al.*, *Phys. Plasmas* **5**, 1446 (1998).
- [16] F. Hattori, H. Takabe, and K. Mima, *Phys. Fluids* **26**, 1719 (1986); H. Sakagami and K. Nishihara, *Phys. Rev. Lett.* **65**, 432 (1990); R.P.J. Town and A.R. Bell, *ibid.* **67**, 1863 (1991); M.M. Marinak *et al.*, *Phys. Plasmas* **3**, 2070 (1996); R. Kishony and D. Shvarts, *ibid.* **8**, 4925 (2001).
- [17] S. Atzeni and A. Caruso, *Nuovo Cimento Soc. Ital. Fis., B* **80**, 71 (1984); *Phys. Lett. A* **85**, 345 (1981).
- [18] V. Lobatchev and R. Betti, *Phys. Rev. Lett.* **85**, 4522 (2000).
- [19] V.A. Smalyuk *et al.*, *Phys. Plasmas* **9**, 2738 (2002).
- [20] S. Haan, *Phys. Fluids B* **3**, 2349 (1991); D. Shvarts *et al.*, *Phys. Plasmas* **2**, 2465 (1995); T. Ikegawa and K. Nishihara, *Phys. Rev. Lett.* **89**, 115001 (2002); J. Sanz *et al.*, *ibid.* **89**, 195002 (2002).
- [21] S. Atzeni, *Comput. Phys. Commun.* **43**, 107 (1986); code upgrades are summarized in S. Atzeni and M.L. Ciampi, *Nucl. Fusion* **37**, 1665 (1997), and references therein.
- [22] R. Betti *et al.*, *Phys. Plasmas* **9**, 2277 (2002).
- [23] J.J. Honrubia, *J. Quant. Spectrosc. Radiat. Transf.* **49**, 491 (1993).
- [24] J.D. Kilkenny *et al.*, *Phys. Plasmas* **1**, 1379 (1994).
- [25] In Figs. 4 and 6 growth rates from DUEE are multiplied by 1.1, to account for estimated code inaccuracy.